ADVANCED MATERIALS INTERFACES
www.advmatinterfaces.de



# Ultralight and Flexible Monolithic Polymer Aerogel with Extraordinary Thermal Insulation by A Facile Ambient Process

*Man Li, Zihao Qin, Ying Cui, Chiyu Yang, Changyu Deng, Yunbo Wang, Joon Sang Kang, Hongyan Xia, and Yongjie Hu**

**High performance thermal insulation materials are desired for a wide range of applications in space, buildings, energy, and environments. Here, a facile ambient processing approach is reported to synthesize a highly insulating and flexible monolithic poly(vinyl chloride) aerogel. The thermal conductivity is measured respectively as 28 mW (m K)$^{-1}$ at atmosphere approaching the air conductivity and 7.7 mW (m K)$^{-1}$ under mild evacuation condition. Thermal modeling is performed to understand the thermal conductivity contributions from different heat transport pathways in air and solid. The analysis based on the Knudsen effect and scattering mean free paths shows that the thermal insulation performance can be further improved through the optimization of porous structures to confine the movement of air molecules. Additionally, the prepared aerogels show superhydrophobicity due to the highly porous structures, which enables new opportunities for surface engineering. Together, the study demonstrates an energy-saving and scalable ambient-processing pathway to achieve ultralight, flexible, and superhydrophobic poly(vinyl chloride) aerogel for thermal insulation applications.**

High performance thermal insulation materials are desired for a wide range of applications in cryogenics, space, subsea systems, buildings, and civil, biomedicines, energy, and environments.[1–4] Traditional insulation materials include porous structures such as fiberglass, mineral wool, cellulose, polyurethane, and polystyrene foams.[5] Aerogel, most commonly based on silica, is an extremely porous structure artificially formed through the careful drying out of the liquid component inside a gel and leaving a solid filled up almost entirely by air.[6] Despite of its record-low thermal conductivity, the fragility, and brittleness of silica aerogel needs to be improved for applications where mechanical strengths are important. Recent progress has been made in developing aerogels involving organic or nanostructured components[7–16] to improve the mechanical properties. However, most synthesis methods usually involve chemical reactions in gel preparation and are limited to specific materials. In addition, the manufacturing cost introduced by delicate processes such as supercritical drying in preparing high-quality aerogels requires high pressure equipment and consumes large amount of liquid carbon dioxide can pose challenge for large scale deployment.

Here, we develop a facile approach to prepare monolithic polymer aerogel based on poly(vinyl chloride) (PVC) via physical processes at ambient environment. Instead of making porous network via crosslink between different molecular chains or covalent bonding between different nanoparticles,[8,17] the porous network is formed by polymer chains entanglement between different precipitated polymer clusters. Taking advantage of the flexibility of polymer, the porous network remains robust while drying at ambient environment and shows a very low thermal conductivity approaching the air conductivity. Combing with the porosity and pressure dependent thermal conductivity, the thermal transport mechanism in PVC aerogel is carefully analyzed. Furthermore, superhydrophobicity is observed in these synthesized high porosity PVC aerogels.

We developed an ambient synthesis process of PVC aerogel mainly consisting of three steps: gelation, solvent exchange, and drying (**Figure 1**a). First, the reaction sources, i.e., PVC powder (389 293, Sigma-Aldrich, USA) is mixed with dimethylformamide (DMF) (DX1727, EMD Millipore, Germany) with ratio from 0.2 g/10 mL to 1 g/10 mL at temperature of 60 °C. The porosity of aerogel is controlled by tuning the concentrations of PVC solutions. Second, the solution is sonicated for an hour and exposed to air for 12 h, from which the water vapor is absorbed into DMF/PVC solution. Consequently, the solubility of PVC decreases gradually resulting in the precipitation of polymer particles. Finally, a white and jelly-liked PVC solid was formed. To remove the liquid from the PVC gel while avoiding shrinkage of the porous structure, the solvent is exchanged with ethanol, which has a small surface tension. The solvent exchange process includes five steps each with a time interval of 6 h to gradually increase the volume percentage of ethanol in the solvent from 0%, 25%, 50%, 75%, 87.5% to 93.8%.

M. Li, Z. Qin, Y. Cui, C. Yang, C. Deng, Y. Wang, J. S. Kang, H. Xia, Prof. Y. Hu
School of Engineering and Applied Science
University of California
Los Angeles (UCLA), Los Angeles, CA 90095, USA
E-mail: yhu@seas.ucla.edu

The ORCID identification number(s) for the author(s) of this article can be found under https://doi.org/10.1002/admi.201900314.

**DOI: 10.1002/admi.201900314**

 

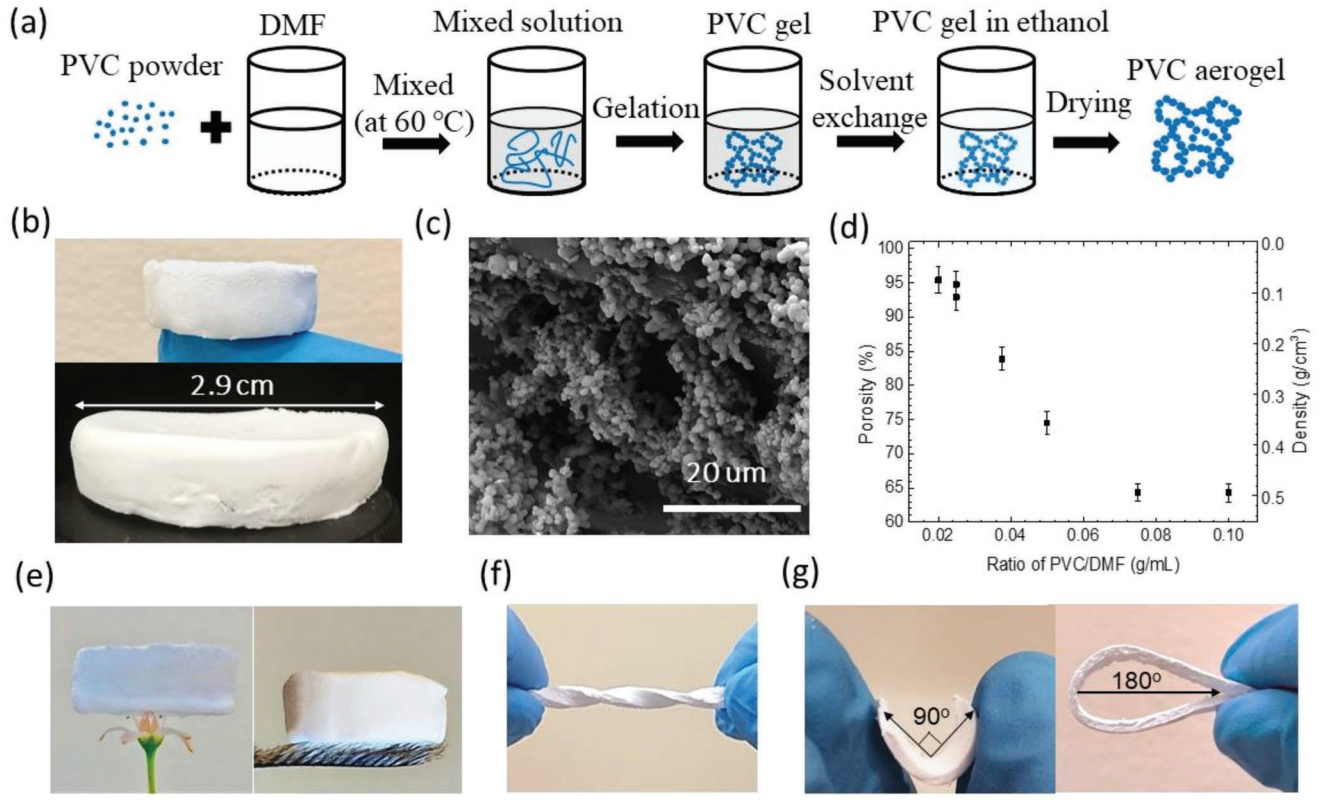


**Figure 1.** Ambient synthesis and characterizations of poly(vinyl chloride) (PVC) aerogels. a) Schematic illustrating the ambient synthesis process. b) Optical image of a typical PVC aerogel sample. c) Scanning electron microscope (SEM) image of PVC aerogel showing a porous network consisting of PVC particles. d) The relationship between the porosity of aerogel and the mass ratio of chemical precursors. e) Ultralight aerogel sample balanced on a flower and a foxtail, f) the twisting test, and g) bending test of the flexible PVC aerogel.

Following aged for twelve hours, the gel is exposed to ambient environment. After the solvent is completely evaporated, a solid backbone is formed as shown in the optical image (Figure 1b). The volume of aerogel can expand by more than ten times larger than that of the original PVC powder indicating a sample with high porosity is formed and filled with air. Note that this ambient processing approach allows readily preparation of inch-size PVC aerogel samples and further scaling up (Figure 1b).

The microscopic structures of PVC aerogel samples were examined using scanning electron microscope (SEM) as shown in Figure 1c. It can be observed that there are enormous PVC particles with diameter from 0.5 to 5 µm connected with each other with necks at the microscale. These PVC particles are initially precipitated during diffusion of water vapor into DMF solvent. While the growth of distributed PVC particles, the dangling polymer chains can entangle with the chains from other particles. Finally, different particles are connected and form a porous network. It was observed that when a small droplet of water was added into the solution, a lot of white PVC particles precipitated but not connected, which proved the critical importance of a natural slow absorption process. It should be noted here this dynamical process of generation of polymer network can happen to other polymers in principle only if the polymers are well dissolved in a certain solvent and precipitated gradually with absorption of insoluble solvent. The effective density $\rho_{\text{eff}}$ can be measured based on Archimedes principle, from which the porosity can be directly derived from the comparison with the density of bulk form PVC ( $\rho_{\text{PVC}} = 1.38\ \text{g cm}^{-3}$) according to the following equation

$$\varnothing = 1 - \frac{\rho_{\text{eff}}}{\rho_{\text{PVC}}} \tag{1}$$

As summarized in Figure 1d, when the ratio of PVC/DMF varies from 0.02 to 0.10 gram per mL, the porosity can change from 60.4% to 95.4% continually, with density decreasing from 0.546 to 0.063 g $\text{cm}^{-3}$. In comparison, such a low mass density of 0.063 g $\text{cm}^{-3}$ corresponds to a porosity of 97% for silica aerogel, which however usually requires delicate synthesis methods such as supercritical drying or multiple surface modifications.[18] The lightness and flexibility of the synthesized PVC aerogel are further illustrated in Figure 1e–g. As an example, a 3.5 cubic centimeter of the PVC aerogel weighs just 230 mg and is so light that it can be balanced on a flower and a blade of foxtail grass (see Figure 1e). In addition, the as-synthesized PVC aerogel can be highly twisted to a rope but without leading to a mechanical breakdown (Figure 1f), which is impossible for standard silica-based aerogels. To further explore the potential application in flexible devices, we have performed a compression test and the PVC aerogel shows high robustness and reversibility for bending at large angles of 90°–180° (Figure 1g). Such an ultraflexibility remains challenging for other aerogels.

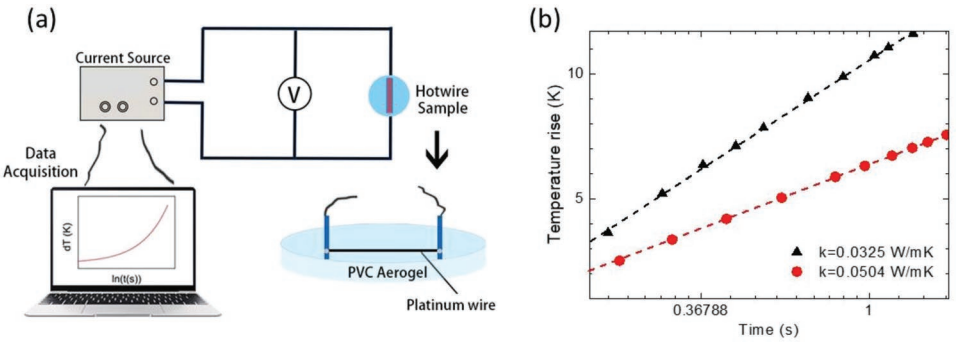


**Figure 2.** Thermal conductivity measurement of PVC aerogels. a) Schematic of hot-wire thermal conductivity measurement. b) Typical experimental data (symbols) fitted to the transient heat conduction model (dash lines). Black and red color represents samples prepared with different initial PVC mass to DMF volume ratios, i.e., here respectively 0.025 and 0.05 g $mL^{-1}$.

Thermal conductivity of PVC aerogels is measured using the hot-wire method.[19] The hot-wire method is a standard technique for measuring a wide range of materials.[20–25] In this method, an electrically resistive metal wire is embedded in the sample, serving as both a line heat source and a temperature sensor, as depicted schematically in **Figure 2**a.[26] A constant current is applied and uniform joule heating is generated along the wire, and the local temperature of the wire is sampled instantly by taking advantage of the linear relationship between temperature and resistance of metal wire. More specifically, in our measurement, a platinum wire with a diameter of 23 µm was placed in the PVC/DMF solution. The platinum wire would be well embedded in the sample while the formation of aerogel. By solving the transient heat conduction model, the temperature rise is found linear with the logarithm value of time and the thermal conductivity can be related with the temperature rise rate by

$$\kappa = \frac{\bar{U}I}{4\pi L}\frac{\Delta \ln(t)}{\Delta T} \tag{2}$$

where $\bar{U}$, $I$, and $L$ are the average voltage drop, current across the wire, and the length of the wire. Figure 2b displays two temperature rise curves versus logarithm time of two typical samples prepared with 0.25 g/10 mL and 0.5 g/10 mL PVC mass to DMF volume ratio. The applied current is 89 mA and the wire length of 1.56 cm. For a fixed heating power, a larger slope of the measurement curve would indicate a smaller thermal conductivity. By comparing the temperature rise curve versus time with a transient heat conduction model, the thermal conductivity of sample can be precisely derived.

With such a high porosity and low intrinsic thermal conductivity of bulk PVC around 0.16 mW (m K)$^{-1}$,[27] thermal conductivity of the PVC aerogel with a porosity of 95.4% was measured to be as low as 0.028 mW (m K)$^{-1}$, approaching the thermal conductivity of air (≈0.026 mW (m K)$^{-1}$),[28] which means our PVC aerogel can act as air-like thermal insulation material. Moreover, evacuation to a mild vacuum of ≈0.01 atm is sufficient to further suppress the gaseous heat transfer and to achieve a thermal conductivity as low as to 0.0077 mW (m K)$^{-1}$. From the comparison of thermal conductivity in air and under evacuation, we can find the air molecules have dominant effects on thermal transport in PVC aerogel and the heat conduction through the PVC backbone is negligible. Note that there are three different thermal transport pathways inside aerogel as illustrated in **Figure 3**a: heat conduction through the solid backbone, heat conduction via the gas molecules filled in the pores, and thermal radiation from the surface of the backbone. Thus, the total thermal conductivity of aerogel ($\kappa$) can be decomposed into three components: solid thermal conductivity ($\kappa_s$), gaseous thermal conductivity ($\kappa_g$), and radiative thermal conductivity ($\kappa_r$), which can be mathematically expresses as[29]

$$\kappa = \kappa_s + \kappa_g + \kappa_r \tag{3}$$

From the heat transfer estimation, the radiative thermal conductivity $\kappa_r$ is less than 0.002 mW (m K)$^{-1}$ when porosity is below 95%,[29] which is much smaller than the other components. Therefore, the two main contributions to thermal transport in the PVC aerogels are $\kappa_s$ and $\kappa_g$, which are affected mostly by the porosity and pore size. Porosity dependent $\kappa$ of PVC aerogels were measured and plotted in Figure 3b. When samples are measured in air, $\kappa$ decreases monotonically from 0.0618 to 0.0283 mW (m K)$^{-1}$ with porosity from 60.4% to 95.4%, indicating that $\kappa_s$ contributes to the heat conduction following the volumetric fractions of the solid PVC backbone.

To make a comparison, literature data of silica aerogel from supercritical drying and ambient drying processes[18,30] are also plotted in Figure 3b. For the same porosity, the PVC aerogel demonstrates remarkably lower thermal conductivity than silica aerogels prepared from both methods. The PVC samples were also measured in mild vacuum at a pressure around 0.001 atm, and show a thermal conductivity from 0.0356 to 0.0077 mW (m K)$^{-1}$ for the same porosity range. For the sample with porosity of 95.4%, the gaseous contribution $\kappa_g$ can be calculated from the subtraction of the thermal conductivity value in vacuum from that in air. This calculation gives $\kappa_g$ to be around 0.0206 mW (m K)$^{-1}$. On the other hand, from the calculation using the porosity and the thermal conductivity of air, $\kappa_g$ is 0.0245 mW (m K)$^{-1}$, which is 20% higher than the former value. We attribute such a difference in $\kappa_g$ to the Knudsen effect[7,17,29,31] of air molecules in confined space, i.e., small pores inside the PVC aerogels. This Knudsen effect indicates that if the pore size is smaller than or comparable with the traveling mean free path of the gas molecules in free space, the gas molecules would collide with the solid framework before their interactive scattering.

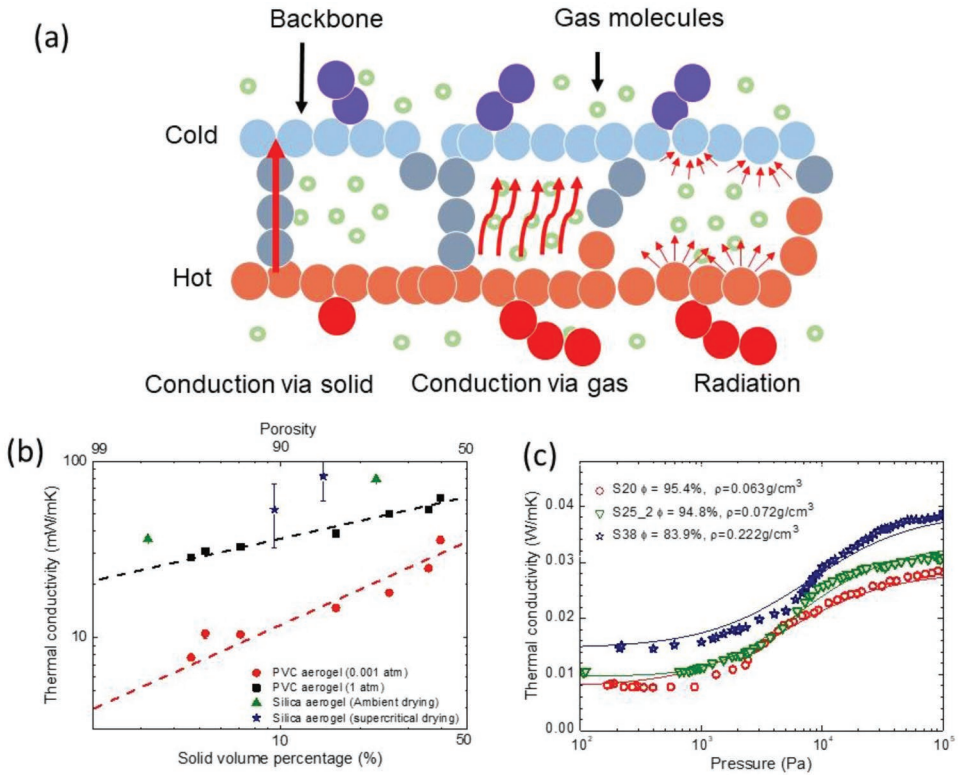


**Figure 3.** Thermal transport analysis in PVC aerogel. a) Thermal transport pathways inside PVC aerogel, consisting of heat conduction through solid backbone, heat conduction via gas molecules, and thermal radiation from surface of backbone. b) Porosity dependent thermal conductivity of PVC aerogel in air and at 0.01 atm. Literature data [18, 30] on thermal conductivity of silica aerogel obtained from supercritical drying and ambient drying are included for comparison. The guidelines are power law fitting of experimental data to illustrate the porosity–thermal conductivity relationship. c) Pressure dependent thermal conductivity of PVC aerogel with different porosities and mass densities. The red, green and blue color represents the PVC aerogel with a porosity of 95.4%, 94.8%, and 83.9%, respectively. The symbols are for experimental data and the lines are for best fittings.

Such additional scattering with solid framework can effectively lower the mean free path of gas molecules than its intrinsic values in free space, and thereby reduce thermal conductivity. Further reduction in pore size will lead to stronger Knudsen effect, and thus lower thermal conductivity.

Here, we use the Knudsen effect to analyze the pore size of the PVC aerogel by measuring their pressure dependent thermal conductivity. The pressure dependent thermal conductivity of high porosity aerogel samples is measured from 100 Pa to ambient pressure (Figure 3c). Note that among the three heat transfer contributions, $\kappa_r$ and $\kappa_s$ are pressure independent, and the decrease of $\kappa$ with reduced pressure represents the reduction of $\kappa_g$. From the kinetic theory, the thermal conductivity of air can be calculated as[32]

$$\kappa_g = A\rho c_V \bar{v} \Lambda \tag{4}$$

where A is a constant, and $\rho, C_V, \bar{v}$, and $\Lambda$ are the air density, specific heat, average velocity, and mean free path of molecules respectively. $\rho$ is proportional to the pressure, and $\Lambda$ is inversely proportional to pressure. Thus, in principle, $\kappa_g$ in free space should be pressure independent. Contrary from the simplification, $\kappa_g$ of PVC aerogel from measurement (Figure 3c) strongly depends on the ambient pressure because the porous structure limits the air molecules diffusion and breaks the inverse relationship between $\Lambda$ and the pressure. The $\Lambda$ of air molecules in a porous structure can be calculated based on Matthiessen's rule[32]

$$\Lambda = \frac{D}{D + \Lambda_0} \Lambda_0 \tag{5}$$

$D$ is pore size in diameter. $\Lambda_0$ is the mean free path of air molecules in free space and is calculated using $\Lambda_0 = \frac{B}{P}$, where $P$ is the pressure in the unit of Pa. Since $\Lambda_0$ equals to 66 nm at 1 atm,[32] $B$ equals to 0.00663 for air. So the total thermal conductivity at different pressures can be calculated as

$$\kappa = \kappa_s + \kappa_{g,0} \frac{PD}{B + PD} \tag{6}$$

where $\kappa_{g,0}$ is the gaseous thermal conductivity at 1 atm. $\kappa_s$ represents the solid state contribution and can be measured at a high pressure (e.g., 100 Pa). From Equation (6), we can find that when the pore size is smaller, $\kappa_g$ would be smaller at a fixed pressure. The experimental data with best fitting using Equation (6) is shown in Figure 3c. For a fixed pore diameter, It is clear that $\kappa$ increases for high pressure since $\kappa_g$ is increasing. The average pore size was extracted from the modeling fitting with experiment and ranges from 800 to 1300 nm. Note that the distribution

**Table 1.** Properties of PVC aerogels prepared with different porosities.

| Sample | PVC [g] | DMF [mL] | Porosity | Mass density [g cm$^{-3}$] | Thermal conductivity in air mW (m K)$^{-1}$ | Thermal conductivity at 0.01 atm mW (m K)$^{-1}$ | Contact angle with water [°] |
|---|---|---|---|---|---|---|---|
| **S20** | 0.20 | 10 | 95.4% | 0.063 | 28.3 | 7.7 | 160.2 |
| **S25_1** | 0.25 | 10 | 92.9% | 0.098 | 32.6 | 10.4 | 158.1 |
| **S25_2** | 0.25 | 10 | 94.8% | 0.071 | 30.9 | 10.5 | 158.0 |
| **S38** | 0.38 | 10 | 83.9% | 0.222 | 38.9 | 14.7 | 147.3 |
| **S50** | 0.50 | 10 | 74.5% | 0.352 | 50.4 | 17.9 | 131.1 |
| **S75** | 0.75 | 10 | 64.3% | 0.493 | 53.1 | 24.7 | 101.4 |
| **S100** | 1.00 | 10 | 60.4% | 0.546 | 61.8 | 35.6 | 97.7 |

of pore sizes provides the substantial confinement to the travelling of molecules despite that the average pore size is larger than the mean free path $\Lambda$ of air molecules at atmosphere pressure,

Next, we explore the superhydrophobicity of the PVC aerogel. The hydrophobic property of a material is determined by the wettability of surface (i.e., the interaction with water). When the Young contact angle on a surface is over 150°, they are defined as superhydrophobic materials.[33–36] Superhydrophobicity can be extremely beneficial for various potential applications.[37] For instance, in building materials involving water-resistance or absorption of hydrophobic substances such as oil.[38] However, classic materials such as silica tend to shrink and cloud in humid environments, and therefore destroy its transparency and integrity. Superphydrophobic surfaces are intensively investigated and specially formulated to repel water and not absorb moisture from the air.[39,40] Here, we perform contact angle measurement and reveal that supershydrophobic PVC aerogels can be achieved at a high porosity. The contact angle of PVC aerogel samples with water are summarized in **Table 1** with the other properties. In comparison, the contact angel of bulk PVC with water of is ≈87°, which indicates a slightly hydrophilic material. Notably, the aerogels samples with porosity higher than 85% have the contact angle over 150°. The tested contact angle is as high as to 160.2° when the porosity increases to 95%, implying a superhydrophobic material. To evaluate the structural stability, these samples were remeasured after being kept in ambient environment for more than a month and still sustain the superhydrophobicity.

We attribute the micropores near the PVC aerogel surface as the main reason for the observed superhydrophobicity, as illustrated in **Figure 4**a. These surface porosity can serve as roughness on a flat surface and create hydrophobic materials.[41] Cassie and Baxter put forward an analytical model for porous solid surface in which no water is filled[41]

$$\cos\theta_c = f\cdot(\cos\theta_{c,0}+1)-1 \tag{7}$$

where $\theta_c$, $\theta_{c,0}$, $f$ are respectively the contact angle between porous surface and water, the contact angle between dense surface and water, and the fraction of solid on the surface. Since the PVC itself is weakly hydrophilic, some space of the pores near the surface would be filled. The wetting status would be a mixed state of Wenzel state and Cassie–Baxter models. For the mixed state, the contact angle can be calculated by combining Equation (7) and Wenzel model[42]

$$\cos\theta_c = f\cdot(r\cdot\cos\theta_{c,0}+1)-1 \tag{8}$$

where $r$ is the roughness factor, defined as the ratio of the actual wetted area to the projected area on the surface.[43] In Figure 4b,

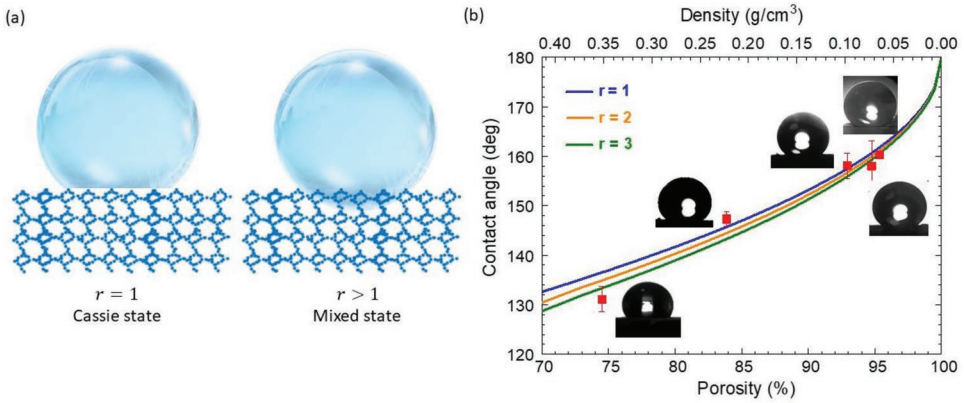


**Figure 4.** Contact angel measurement and superhydrophobicity of PVC aerogels. a) Schematic illustrating the mechanism how the surface porosity improves the surface area and the contact angle with water. b) The porosity dependent contact angle of PVC aerogel, following the prediction based on Cassie–Baxter model (blue) and Wenzel model (orange and green). $r$ is the roughness factor, defined as the ratio of the actual wetted area to the projected area on the surface.

the predicted contact angles for aerogel with different porosities are plotted together with the experimental data. The experimental measurement of contact angles are plotted together with the calculation in Figure 4b, and shows good agreement, indicating that the high porosity of PVC aerogel increases gas-solid interface areas and enhances the surface roughness, which together leads to the superhydrophobicity. The observed superhydrophobicity in the PVC aerogels synthesized by this facile ambient process can enable new opportunities in designing water-repelling building blocks, surface engineering, and drug delivery platforms.[44–47]

In summary, we develop a facile method to synthesize ultralight and flexible polymer aerogel with low thermal conductivity without supercritical drying. We successfully prepared PVC aerogels with the porosities ranging from 60% to 95% and measured the thermal conductivity of the PVC aerogel as 28 mW (m K)$^{-1}$ in air and 7.7 mW (m K)$^{-1}$ under mild evacuation. The contribution from air conduction dominates the thermal transport in PVC aerogel. Our modeling analysis indicates that the lower boundary of thermal conductivity can be pushed by further reducing the pore size and increase the porosity. In addition, we measured the contact angle of PVC aerogel with water and found that the PVC aerogels with porosity larger than 85% are superhydrophobic. The porosity-dependent contact angles from experimental measurement are in good consistence with theory prediction by mixed Cassie–Baxter and Wenzel models. The low thermal conductivity, mechanical flexibility, and superhydrophobicity show high promise in engineering the PVC aerogel for thermal management applications[48,49] under different working environments.

## Supporting Information

Supporting Information is available from the Wiley Online Library or from the author.

## Acknowledgements

Y.H. acknowledges support from an Alfred P. Sloan Research Fellowship, a CAREER award through the National Science Foundation, a Young Investigator Award through the U.S. Air Force Office of Scientific Research, a Doctoral New Investigator Award from American Chemical Society Petroleum Research Fund, the UCLA Sustainable LA Grand Challenge, and the Anthony and Jeanne Pritzker Family Foundation.

## Conflict of Interest

The authors declare no conflict of interest.

## Keywords

aerogels, ambient process, flexible, low thermal conductivity, poly(vinyl chloride), superhydrophobicity, thermal insulation

Received: February 18, 2019
Revised: April 16, 2019
Published online: May 27, 2019

[1] United States Department of Energy. Insulation Materials https://www.energy.gov/energysaver/weatherize/insulation/insulation-materials (accessed: December 2018).
[2] N. P. Padture, M. Gell, E. H. Jordan, *Science* **2002**, *296*, 280.
[3] B. P Jelle, *Energy Build.* **2011**, *43*, 2549.
[4] M. S. Dresselhaus, G. Chen, M. Y. Tang, R. Yang, H. Lee, D. Wang, Z. Ren, J. P. Fleurial, P. Gogna, *Adv. Mater.* **2007**, *19*, 1043.
[5] A. M. Papadopoulos, *Energy Build.* **2005**, *37*, 77.
[6] S. S. Kistler, *Nature* **1931**, *127*, 741.
[7] X. Lu, M. C. Arduini-Schuster, J. Kuhn, O. Nilsson, J. Fricke, R. W. Pekala, *Science* **1992**, *255*, 971.
[8] J. L. Mohanan, I. U. Arachchige, S. L. Brock, *Science* **2005**, *307*, 397.
[9] F. Qian, P. C. Lan, M. C. Freyman, W. Chen, T. Kou, T. Y. Olson, C. Zhu, M. A. Worsley, E. B. Duoss, C. M. Spadaccini, T. Baumann, T. Y. Han, *Nano Lett.* **2017**, *17*, 7171.
[10] F. Guo, Y. Jiang, Z. Xu, Y. Xiao, B. Fang, Y. Liu, W. Gao, P. Zhao, H. Wang, C. Gao, *Nat. Commun.* **2018**, *9*, 881.
[11] S. M. Jung, H. Y. Jung, M. S. Dresselhaus, Y. J. Jung, J. Kong, *Sci. Rep.* **2012**, *2*, 849.
[12] M. B. Bryning, D. E. Milkie, M. F. Islam, L. A. Hough, J. M. Kikkawa, A. G. Yodh, *Adv. Mater.* **2007**, *19*, 661.
[13] H. Sun, Z. Xu, C. Gao, *Adv. Mater.* **2013**, *25*, 2554.
[14] A. Cao, *Science* **2005**, *310*, 1307.
[15] Z. Chen, W. Ren, L. Gao, B. Liu, S. Pei, H. M. Cheng, *Nat. Mater.* **2011**, *10*, 424.
[16] S. Nardecchia, D. Carriazo, M. L. Ferrer, M. C. Gutiérrez, F. del Monte, *Chem. Soc. Rev.* **2013**, *42*, 794.
[17] X. Lu, P. Wang, M. C. Arduini-Schuster, J. Kuhn, D. Büttner, O. Nilsson, U. Heinemann, J. Fricke, *J. Non-Cryst. Solids* **1992**, *145*, 207.
[18] T. Y. Wei, T. F. Chang, S. Y. Lu, Y. C. Chang, *J. Am. Ceram. Soc.* **2007**, *90*, 2003.
[19] M. J. Assael, K. D. Antoniadis, W. A. Wakeham, *Int. J. Thermophys.* **2010**, *31*, 1051.
[20] D. Wen, Y. Ding, *J. Thermophys. Heat Transfer* **2004**, *18*, 481.
[21] J. J. Healy, J. J. De Groot, J. Kestin, *Physica B+C* **1976**, *82*, 392.
[22] L. C. Wei, L. E. Ehrlich, M. J. Powell-Palm, C. Montgomery, J. Beuth, J. A. Malen, *Addit. Manuf.* **2018**, *21*, 201.
[23] R. Zheng, J. Gao, J. Wang, G. Chen, *Nat. Commun.* **2011**, *2*, 289.
[24] D. W. Stops, *Nature* **1949**, *164*, 966.
[25] N. A. Rongione, M. Li, H. Wu, H. D. Nguyen, J. S. Kang, B. Ouyang, H. Xia, Y. Hu, *Adv. Electron. Mater.* **2019**, *5*, 1800774.
[26] E. Cohen, L. Glicksman, *J. Heat Transfer* **2014**, *136*, 041301.
[27] K. Eiermann, K. Hellwege, *J. Polym. Sci.* **1962**, *57*, 99.
[28] R. B. Montgomery, *J. Meteorol.* **1947**, *4*, 193.
[29] L. W. Hrubesh, R. W. Pekala, *J. Mater. Res.* **1994**, *9*, 731.
[30] P. E. Hopkins, B. Kaehr, E. S. Piekos, D. Dunphy, J. Brinker, *J. Appl. Phys.* **2012**, *111*, 113532.
[31] G. H. Tang, C. Bi, Y. Zhao, W. Q. Tao, *Energy* **2015**, *90*, 701.
[32] W. Woodside, J. H. Messmer, *J. Appl. Phys.* **1961**, *32*, 1688.
[33] J. Drelich, E. Chibowski, D. D. Meng, K. Terpilowski, *Soft Matter* **2011**, *7*, 9804.
[34] K. Koch, W. Barthlott, *Philos. Trans. R. Soc., A* **2009**, *367*, 1487.
[35] I. Karapanagiotis, P. N. Manoudis, A. Zurba, D. Lampakis, *Langmuir* **2014**, *30*, 13235.
[36] J. Drelich, A. Marmur, *Surf. Innovations* **2014**, *2*, 211.
[37] T. Darmanin, F. Guittard, *Mater. Today* **2015**, *18*, 273.
[38] X. Yao, J. Gao, Y. Song, L. Jiang, *Adv. Funct. Mater.* **2011**, *21*, 4270.
[39] T. Liu, C.-J. Kim, *Science* **2014**, *346*, 1096.
[40] T. S. Wong, S. H. Kang, S. K. Y. Tang, E. J. Smythe, B. D. Hatton, A. Grinthal, J. Aizenberg, *Nature* **2011**, *477*, 443.
[41] A. B. D. Cassie, S. Baxter, *Trans. Faraday Soc.* **1944**, *40*, 546.

 

[42] R. N. Wenzel, *Ind. Eng. Chem.* **1936**, *28*, 988.
[43] E. Bormashenko, *Adv. Colloid Interface Sci.* **2015**, *222*, 92.
[44] D. A. Doshi, P. B. Shah, S. Singh, E. D. Branson, A. P. Malanoski, E. B. Watkins, J. Majewski, F. van Swol, C. J. Brinker, *Langmuir* **2005**, *21*, 7805.
[45] I. Smirnova, J. Mamic, W. Arlt, *Langmuir* **2003**, *19*, 8521.
[46] A. Lendlein, R. B. Langer, *Science* **2002**, *296*, 1673.
[47] J. Ge, L.-A. Shi, Y.-C. Wang, H.-Y. Zhao, H.-B. Yao, Y.-B. Zhu, Y. Zhang, H.-W. Zhu, H.-A. Wu, S.-H. Yu, *Nat. Nanotechnol.* **2017**, *12*, 434.
[48] J. S. Kang, M. Li, H. Wu, H. Nguyen, Y. Hu, *Science* **2018**, *361*, 575.
[49] J. S. Kang, H. Wu, Y. Hu, *Nano Lett.* **2017**, *17*, 7507.

 